Received: 15 December 2019 | Revised: 8 March 2020 | Accepted: 20 March 2020

DOI: 10.1002/ese3.706

RESEARCH ARTICLE

Energy Science & Engineering
Open Access

Design of a novel hybrid control strategy for multi-inverter parallel system for resonance suppression

Feng Zheng[1] | **Xiangqun Lin**[1] | **Yachao Zhang**[1] | **Changhong Deng**[2]

[1]School of Electrical Engineering and Automation, Fuzhou University, Fuzhou, China

[2]School of Electrical Engineering and Automation, Wuhan University, Wuhan, China

Correspondence
Changhong Deng, School of Electrical Engineering and Automation, Wuhan University, Wuhan, China.
Email: dengch-whu@163.com

Funding information
This work was supported in part by Natural Science Foundation of Fujian Province, China (2019J01249), and in part by the National Key R&D Program of China under Grant (2017YFB0902200).

Abstract

Comparing with the *LCL*-type single-inverter parallel system, the multi-inverter parallel system has more complex resonance characteristics which are generated by three type resonance sources (reference current changing in the inverter control system, reciprocal effect among multi-inverters and grid background harmonic) and cause great negative effects on power system. In order to suppress the resonance problem of *LCL*-type multi-inverters parallel system, a novel control strategy is proposed in this paper based on model current predictive control (MCPC) and two-degree-of-freedom control. Through MCPC, this strategy can reduce the number of current inner-loop PI of control layer and remove PWM module. Then, a potential robustness can be obtained. From the outer loop of control layer perspective, because MCPC's value function consists of inverter's output current and reference current of control layer inner loop, they can be approximately regarded as equal. And then through constructing the inverse model of control object, the two-degree-of-freedom control can be introduced to realized transfer function unitarization of control layer's outer loop, so that the order difference between numerator's highest order term and denominator's highest order term of inverter resonance transfer function can be reduced. Accordingly, it can be found that with the three type resonance sources, there is no peak value in their resonance transfer functions and their gains all present attenuation effects. Therefore, the resonance problems of multi-inverter parallel system can be eliminated. Through the theoretical derivation and simulation results, it can be proved that the proposed method can not only enhance the transient performance of multi-inverter parallel system, but also its resonance problems.

KEYWORDS

model current predictive control, multi-inverter parallel system, resonance characteristics, two-degree-of-freedom control, value function

[Correction added on 25 June 2020, after first online publication: The correspondence address was corrected.]

1 | INTRODUCTION

In the past decades, renewable energy sources like wind turbines or photovoltaic systems have gained more and more importance. Therefore, distributed generations (DGs) have developed rapidly.[1-4] In practice, DGs are usually combined into a microgrid or DG subnetworks. It means multiple DGs are connected to grid in parallel mode.[5]

At present, DGs are normally connected to power system by grid-connected inverters. If these grid-connected inverters are directly accessed to power system, there will be abundant harmonics delivered into power system in the form of inverter's output current.[6] For reducing the total harmonic distortion (THD) of inverter's output current, filters are usually adopted. Because *LCL*-type filter has better high-frequency ripple suppression effect and smaller inductance value, they are widely used in the world.[7] However, *LCL*-type filter is a third-order system which can make its transfer function has a resonance peak. Thus, if there is no enough damping to inhibit the peak of its high-frequency resonance, it will generate negative effects on the power system's stability.[8] And when multiple inverters are parallel access to microgrid or DG subnetworks, because of the reciprocal effects among their *LCL*-type filters, the resonance problem of the grid-connected inverters become more complex.[9]

The resonance problems of multi-inverter parallel system are mainly divided into three categories, namely inverter internal resonance, multi-inverter parallel resonance, and grid background harmonic series resonance. For removing these resonance problems, the passive damping and active damping are the most widely used methods. Passive damping method is mainly adopted to increase the system's damping coefficient by series or parallel resistance on the filter's inductor/capacitor component.[10-13] And its advantages and disadvantages can be found referring to.[10] Among them, the method which the resistance is connected in series to filter's capacitor is the best method for suppressing inverter's resonance. And its superior effect has been also proved in.[11-13] However, the large power loss of damping resistor lowers inverter's utilized efficiency. For reducing the power loss of damping resistor, a split-capacitor passive damping control method is proposed in.[14] Nonetheless, this method requires the transformation of the hardware circuit of the filter. In,[15-17] three kinds of active damping methods (inverter side inductor current feedback, filter capacitor voltage feedback, and filter capacitor current feedback) have been proposed to inhibit inverter's resonances. Through increasing zero point of control system's transfer function to enhance damping coefficient of resonance peak, all of them have better resonance suppression effects. However, when the impedance of the power grid changes, the active damping performance of the capacitor current feedback will become worse and the system may even lose stability,[18] so that its robustness will be confined. Another type of the active damping method is to add digital filters (namely low-pass filter, lead-lag filter, and notch filter) in the inverter control system's forward path.[19-21] By changing filter's parameters, the low-pass filter can change the crossing point of the phase curve. Then, it can attenuate the resonance peak to a certain extent.[19] The effect of lead-lag filter is similar to low-pass filter. It can also change the crossing point of the phase curve. Moreover, the lead of the phase can be realized by lead-leg filter.[20] The notch filter can greatly attenuate the resonance peak, and through adding a pair of zero points at the resonance frequency, it can also cancel the inherent resonance under damped resonance pole of LCL. And then, the damping characteristic of the system can be changed.[21] However, this kind of active damping method needs accurate system parameter information (such as filter resonance frequency). Therefore, its robustness is obviously insufficient. Although adding online system parameter identification method may improve control system's robustness, it can still affect the system's power quality.[21]

In addition to the above two types of increasing damping coefficient methods, the grid-side voltage full feedforward method is proposed to suppress the resonance caused by power system background harmonics in.[22] However, this method cannot suppress inverter's internal resonance and multiple inverters' parallel resonance. In,[23] through introducing current feedback for PR current control, the third-order model of *LCL*-type filter is transformed to a first-order model for suppressing inverter's resonance. However, dynamic delays character of PR controller can also affect inverter's robust performance as well as active damping method. In,[24] inverter impedance is reshaped by second-order-generalized-integrator, so that inverter's resonance caused by microgrid's high-frequency harmonics can be suppressed. Nevertheless, reshaping inverter impedance may influence the tracking accuracy of inverter's output power. Through constructing the cancelation function between zero and resonant pole points, a pole-zero configuration strategy is proposed to inhibit inverter's resonance in.[25] However, this method needs complicated mathematics processes. And if there is deviation between zero and resonant pole points, the suppression effects of inverter's resonance will be affected. Therefore, it is necessary to propose a new method which has simple structure, superior robust performances, and excellent resonance suppression effects.

Considering the above research shortage, a novel method is proposed for eliminating resonance of multi-inverter parallel system in this paper, which mainly consists of MCPC and two-degree-of-freedom control. Through MCPC, the number of current inner-loop PI of control layer and PWM module can be removed, so that the fast dynamic response and provides a potential robustness can be obtained. And from the outer loop of control layer perspective, the transfer function of inverter's output current and reference current can be approximatively regarded as equal by the MCPC's action. In outer loop of control layer, the two-degree-of-freedom control is introduced to realized transfer function unitarization. Therefore, the order difference between numerator's highest order term

and denominator's highest order term of inverter resonance transfer function can be reduced. Accordingly, facing the three type resonance sources, there are no peak values in their resonance transfer functions and their gains all present attenuation effects. Therefore, the resonance problems of multi-inverter parallel system can be eliminated.

2 | MULTIGRID INVERTER SYSTEM WITH TRADITIONAL CONTROL METHOD

2.1 | Multigrid inverter modeling

Figure 1 shows the traditional control block diagram of three-phase inverter grid-connected structure including double loop control.[26,27] According to Figure 1, $U(s)$, $U_c(s)$, $I_c(s)$, and $I_g(s)$ can be expressed as follows:

$$\begin{cases} U(s)=AU_c(s)+BI_g(s)-BI_{g\_ref}(s) \\ U_c(s)=CU(s)-CU_c(s)-DI_g(s) \\ I_c(s)=FU_c(s) \\ I_g(s)=EU_c(s)-EU_g(s) \end{cases} \tag{1}$$

Here

$$\begin{cases} A=\begin{bmatrix} -K_{pwm}K_cCs & 0 \\ 0 & -K_{pwm}K_cCs \end{bmatrix} \\ B=\begin{bmatrix} -K_{pwm}G_{PR}(s) & 0 \\ 0 & -K_{pwm}G_{PR}(s) \end{bmatrix} \\ C=\begin{bmatrix} \frac{1}{L_{in}Cs^2} & 0 \\ 0 & \frac{1}{L_{in}Cs^2} \end{bmatrix}, D=\begin{bmatrix} \frac{1}{Cs} & 0 \\ 0 & \frac{1}{Cs} \end{bmatrix}, E=\begin{bmatrix} \frac{1}{L_gs} & 0 \\ 0 & \frac{1}{L_gs} \end{bmatrix} \\ F=\begin{bmatrix} Cs & 0 \\ 0 & Cs \end{bmatrix}, \quad G_{PR}(s)=K_P+\frac{2K_R\omega_cs}{s^2+2\omega_cs+\omega_0^2} \end{cases} \tag{2}$$

$U(s)$ and $U_c(s)$ are inverter's output voltage and filter's capacitor voltage, respectively. I_g, I_c, and I_{g_ref} are grid-connected current, filter's capacitor current, and reference current, respectively. G_{PR} is PR controller. K_{pwm} is inverter's equivalent gains. L_{in} and L_g are filter inductances. C is filter capacitance. K_c is the capacitor current feedback coefficient. Based on Figure 1 and (1), inverter's Norton equivalent model can be shown as Figure 2.

Here, G_i is the control coefficient of the controlled source. Y_i and Y_T are the inverter's output equivalent admittance and gird equivalent admittance. I_g^* is the inverter's output reference current. u_g is the voltage of power system. And according to Figure 1 and (1), the coefficients of the Norton equivalent model can be expressed as:

$$\begin{cases} G_i(s)=\dfrac{K_{pwm}G_{PR}(s)}{C(s)} \\ Y_i(s)=\dfrac{L_{in}Cs^2+K_{pwm}K_cC\cdot s+1}{C(s)} \\ C(s)=L_{in}L_gC\cdot s^3+K_{pwm}K_cL_gC\cdot s^2 \\ \qquad +(L_{in}+L_g)s+K_{pwm}G_{PR}(s) \end{cases} \tag{3}$$

Therefore, according to Figure 2 and superposition theorem, if there were multiple inverters connected to the grid in parallel, their equivalent model can be seen in Figure 3

From Figure 3, the grid-connected current expression of the ith inverter can be obtained by node voltage method and it can be expressed as:

$$\begin{cases} I_{si}(s)=R_i(s)I_{si}^*(s)+I_{st}^*\sum\limits_{t=1,t\neq i}^{n}P_{i,t}(s)-S_{gi}(s)U_g(s) \\ R_i(s)=\dfrac{\sum\limits_{j\neq i}^{n}Y_j(s)+Y_T(s)}{\sum\limits_{i=1}^{n}Y_i(s)+Y_T(s)}G_i(s) \\ P_{i,t}(s)=\dfrac{-Y_i(s)G_t(s)}{\sum\limits_{i=1}^{n}Y_i(s)+Y_T(s)}, t\in[2,n] \\ S_{gi}(s)=\dfrac{Y_i(s)Y_T(s)}{\sum\limits_{i=1}^{n}Y_i(s)+Y_T(s)} \end{cases} \tag{4}$$

Here, Y_i and G_i are the ith inverter's output equivalent admittance and its equivalent controlled source's control

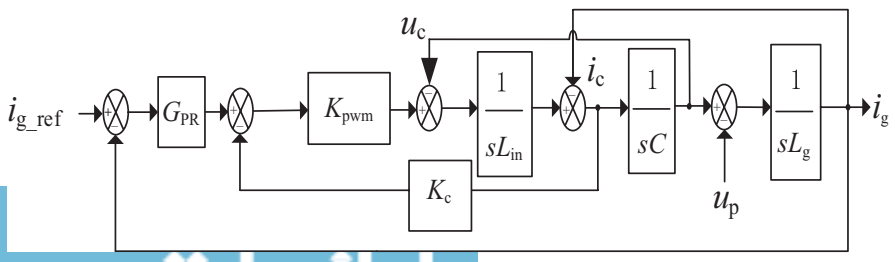

FIGURE 1 Control block diagram of three-phase inverter

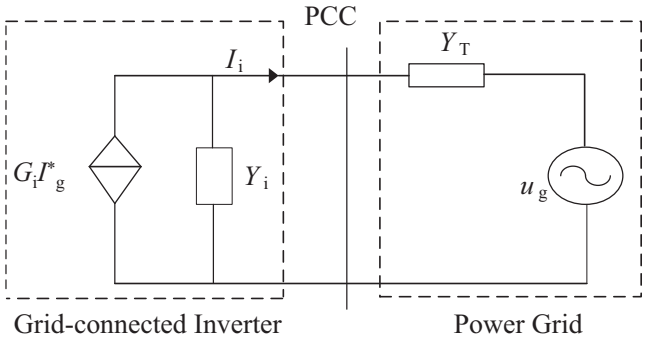

FIGURE 2 Norton equivalent model of inverter

coefficient ($i = 1, 2\ldots, n$), respectively. I_{si} and I^*_{gi} is the ith inverter's output current and its reference value, respectively.

According to (4), the ith inverter's output current, I_{si}, mainly contains three excitations, namely inverter's own excitation, other inverters' excitation, and grid power's excitation. Therefore, the resonance problems of multi-inverter parallel systems can be divided into three categories which are inverter's internal resonance, multi-inverters parallel resonance, and power grid's series resonance.

2.2 | Multi-inverter internal resonance analysis

For facilitating analysis, the first inverter is seen as an example. Then, the transfer function of its internal resonance is

$$R(s)=\frac{I_{s1}(s)}{I^*_{s1}}=\frac{(n-1)Y_1(s)+Y_T(s)}{nY_1(s)+Y_T(s)}G_1(s) \tag{5}$$

Here, n is the number of inverters. According to (5), Figure 4 shows the Bode diagram of the first inverter's internal resonance. From Figure 4, when the number of inverters is greater than one, there are two resonance peaks in the first inverter's internal resonance curve and the gain of high-frequency resonance is larger than the gain of low-frequency resonance. With the number of inverters increasing, the resonance peaks of high-frequency band remain unchanged, but resonance peaks of low-frequency band move in the direction of low frequencies.

To analyze the interaction between inverters on their resonance characteristics, the second inverters are also adopted. Then, the transfer function of their parallel resonance can be expressed as:

$$P_{1,t}(s)=\frac{I_{s1}}{I_{s2}}=\frac{-Y_1(s)G_2(s)}{nY_2(s)+Y_T(s)} \tag{6}$$

According to (6), Figure 5 shows multi-inverter's parallel resonance Bode diagram. From Figure 5, there are also two resonance peaks in resonance curve. And other characteristics of their resonance curve are the same as inverter's internal resonance.

The series resonance's transfer function between the output current of first inverter and voltage of power grid is

$$S_{g1}(s)=\frac{I_{s1}(s)}{U_g(s)}=-\frac{Y_1(s)\cdot Y_T(s)}{nY_i(s)+Y_T(s)} \tag{7}$$

According to (7), Figure 6 shows series resonance Bode diagram of the output current of first inverter and voltage of power grid. According to Figure 6, there is only resonance peak in each resonance curve. And with the number of inverters increasing, the resonance peak will move toward the low-frequency band.

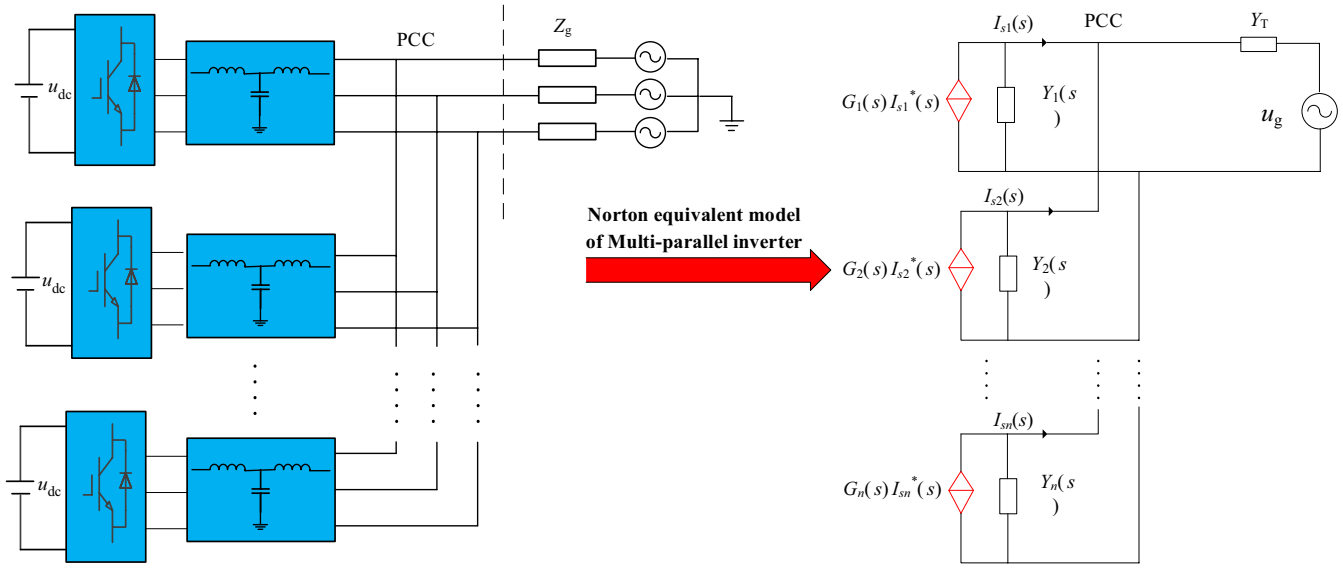

FIGURE 3 Equivalent model of multi-inverter parallel system

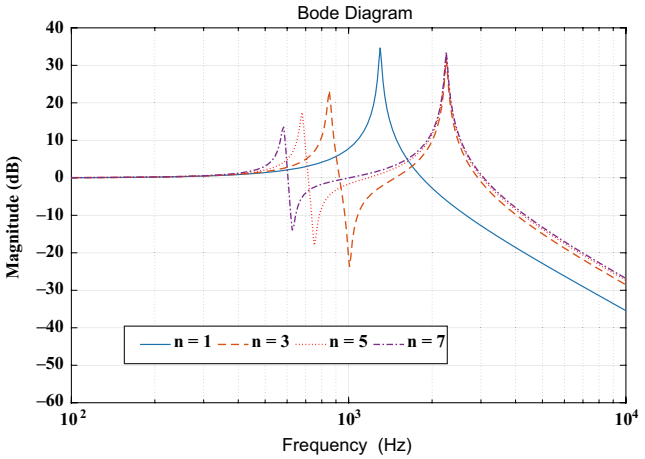

FIGURE 4 Internal resonance Bode diagram of multi-inverter parallel system

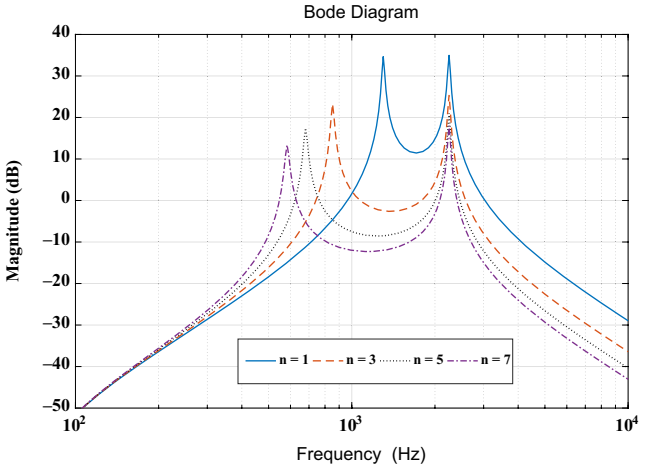

FIGURE 5 Serial resonance Bode diagram of inverter parallel system

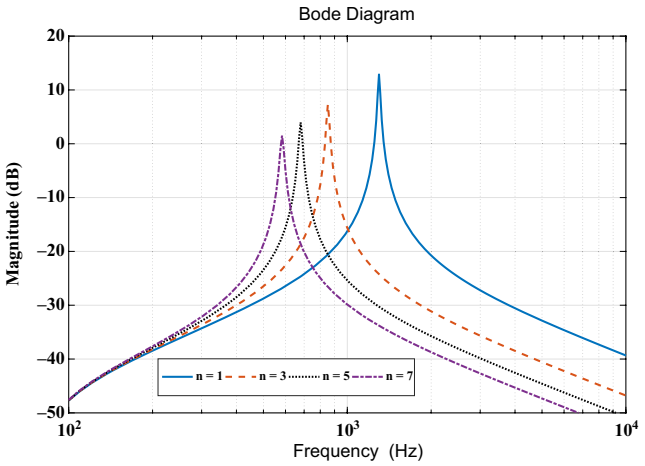

FIGURE 6 Power system background harmonic series resonance Bode diagram

3 | SUPPRESSING MULTI-INVERTER RESONANCE WITH NOVEL CONTROL METHOD

In,[28] the two-degree-of-freedom control method was adopted to unitize the transfer function of control layer. However, there was pure differential element in current inner loop of control layer. In that case, when the inverter coped with the above three type resonances, the stability of its control system would be greatly affected. Therefore, for removing the influences from pure differential element, MCPC is adopted to replace two-degree-of-freedom controller in the current inner loop of control layer. Nevertheless, the two-degree-of-freedom controller in voltage outer loop of control layer is still unchanged, so that the control layer's robustness can be also enhanced.

3.1 | Design of control layer inner loop

Figure 7 shows MCPC system's block diagram.[29] Here, $r(k)$ and $y(k)$ are the input and output signals at time k, respectively. According to Figure 7, the transfer functions between $r(k)$ and $y(k)$ is

$$y(k+1)=ABx(k)+ACr(k) \tag{8}$$

Here, C and A are transfer functions. B is the feedback controller. $1/Z$ is time delay element. If $r(k)$ and $y(k)$ are multidimensional variables, then

$$\begin{cases} y_1(k+1)=ABx(k)+ACr_1(k) \\ \quad\vdots \\ y_i(k+1)=ABx(k)+ACr_i(k) \quad (i=1,\cdots,n) \\ \quad\vdots \\ y_n(k+1)=ABx(k)+ACr_n(k) \end{cases} \tag{9}$$

Therefore, according to (9) and $r_i(k)$, $y_i(k+1)$ can be obtained. For tracking the reference value $y_i^*(k+1)$ accurately, the value function f_i is introduced, so that f_i can be expressed as follows:

$$f_i=\left[y_i^*(k+1)-y_i(k+1)\right]^2 \tag{10}$$

Substituting (9) into (10), the minimum value function can be expressed as follows:

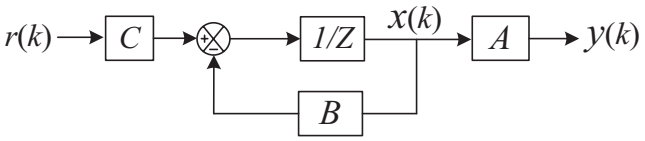

FIGURE 7 Block diagram of MCPC system

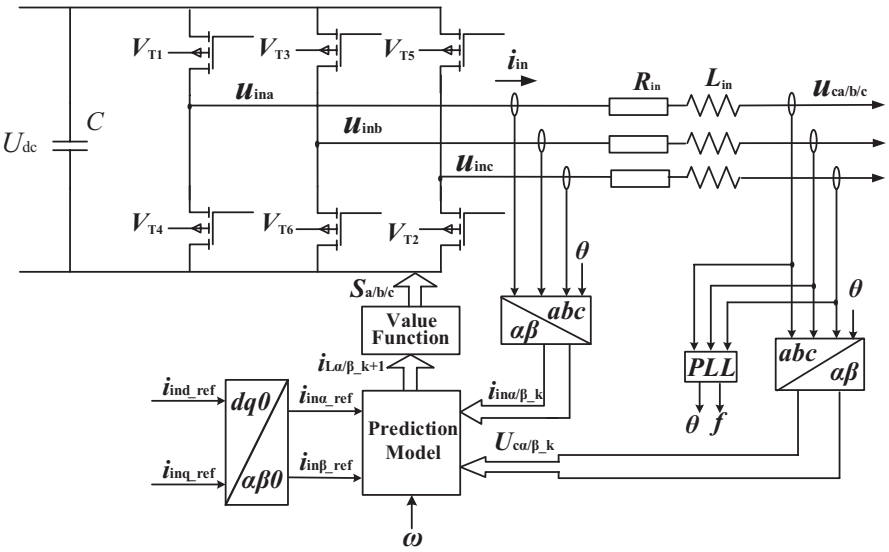

FIGURE 8 Inner-loop schematic diagram of inverter control layer

$$f_{\min} = \min(f_1, \cdots, f_n) \tag{11}$$

Then, $y_i(k+1)$ corresponding to $f_{\min}$ can be adopted for the control system.

Figure 8 shows the inner-loop schematic diagram of inverter's control layer. From Figure 8, together with transformation of *abc* to $\alpha\beta$, AC-side two-phase decoupled circuits of the grid-connected inverter can be obtained as follows[30]:

$$\begin{cases} L_{in}\dfrac{di_{in\alpha}}{dt} = u_{in\alpha} - u_{c\alpha} - R_{in}i_{in\alpha} \\ L_{in}\dfrac{di_{in\beta}}{dt} = u_{in\beta} - u_{c\beta} - R_{in}i_{in\beta} \end{cases} \tag{12}$$

And the inverter output voltage can be expressed as follows:

$$\begin{cases} u_{in\alpha} = \sqrt{\dfrac{2}{3}}\left(g_a - \dfrac{1}{2}g_b - \dfrac{1}{2}g_c\right)U_{dc} \\ u_{in\beta} = \dfrac{\sqrt{2}}{2}(g_b - g_c)U_{dc} \end{cases} \tag{13}$$

TABLE 1 Relationship between switching states and output voltage component

State	g_a	g_b	g_c	u_α	u_β
S_1	0	0	0	0	0
S_2	0	0	1	$0.8165U_{dc}$	0
S_3	0	1	0	$0.4083U_{dc}$	$0.7071U_{dc}$
S_4	0	1	1	$0.4083U_{dc}$	$0.7071U_{dc}$
S_5	1	0	0	$0.8165U_{dc}$	$0U_{dc}$
S_6	1	0	1	$0.4083U_{dc}$	$0.7071U_{dc}$
S_7	1	1	0	$0.4083U_{dc}$	$0.7071U_{dc}$
S_8	1	1	1	0	0

If (12) is discretized at the time of (t_k, t_{k+1}), it can be amended as follows:

$$\begin{cases} i_{in\alpha\_(k+1)} = \dfrac{T_s(u_{in\alpha\_k} - R_{in}L_{in}i_{in\alpha\_k} - u_{c\alpha\_k})}{L_{in}} + i_{in\alpha\_k} \\ i_{in\beta\_(k+1)} = \dfrac{T_s(u_{in\beta\_k} - R_{in}L_{in}i_{in\beta\_k} - u_{g\beta\_k})}{L_{in}} + i_{in\beta\_k} \end{cases} \tag{14}$$

From (13), $u_{in\alpha}/u_{in\beta}$ are controlled by g_a, g_b, and g_c. Table 1 gives three-phase inverter eight switching modes and the

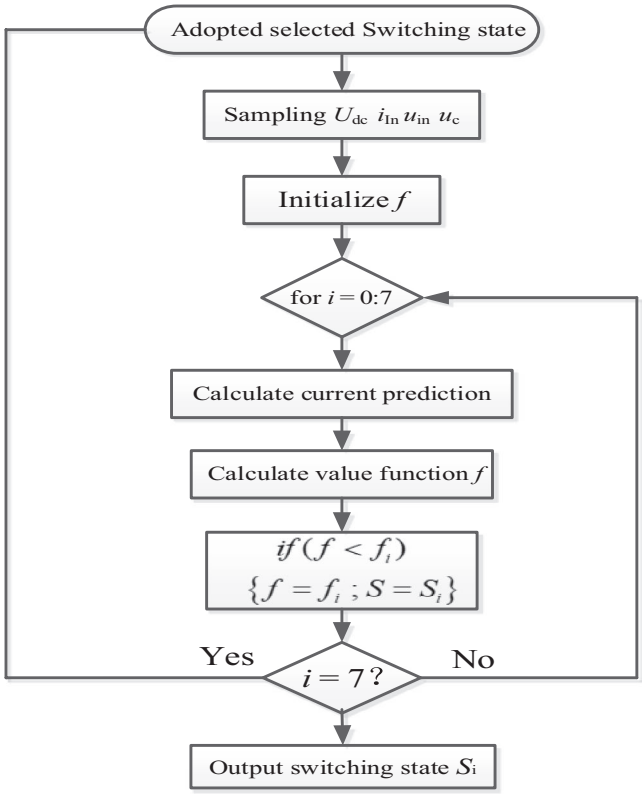

FIGURE 9 Flow diagram of implemented MCPC system

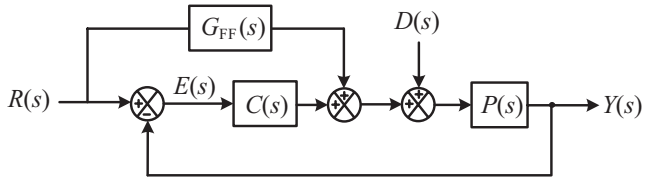

FIGURE 10 Block diagram of the two-degree-of-freedom control

relationships between these switching modes and their output voltages. According to Table 1 and (13), each set of switching modes corresponds to different values of $u_{in\alpha}$ and $u_{in\beta}$. If the voltage values corresponding to the eight switching modes at time k are, respectively, substituted into (14), eight different predicted results for the output current, $i_{in\alpha\text{-}k+1}/i_{in\beta\text{-}k+1}$, can be obtained. If inverter output current is set as the control objective for its control system, the value function f_i can be expressed as follows:

$$\begin{cases} f_{i\_1} = (i_{in\alpha\_ref} - i_{in\alpha 1\_(k+1)})^2 + (i_{in\beta\_ref} - i_{in\beta 1\_(k+1)})^2 \\ \vdots \\ \vdots \\ f_{i\_7} = (i_{in\alpha\_ref} - i_{in\alpha 7\_(k+1)})^2 + (i_{in\beta\_ref} - i_{in\beta 7\_(k+1)})^2 \end{cases} \tag{15}$$

Here, $i_{in\alpha\text{-}ref}$ and $i_{in\beta\text{-}ref}$ are reference currents in the $\alpha\beta$ coordinate frame. Therefore, $f_{\min}$ can be obtained by substituting (12) into (10). Then, g_a, g_b, and g_c corresponding to $f_{\min}$ will be implemented by the grid-connected inverter.

To elucidate the MCPC algorithm for the DC/AC converter controller further, Figure 9 shows a flow diagram of the MCPC algorithm, which was implemented in MATLAB. From Figure 9, the control loop begins sampling the voltage and current signals. Then, the algorithm estimates the grid-connected current by means of (13) and (15) and initializes the value of f, which is a variable that will contain the value of the lowest quality function evaluated by the algorithm so far. Then, the strategy enters a loop where, for each

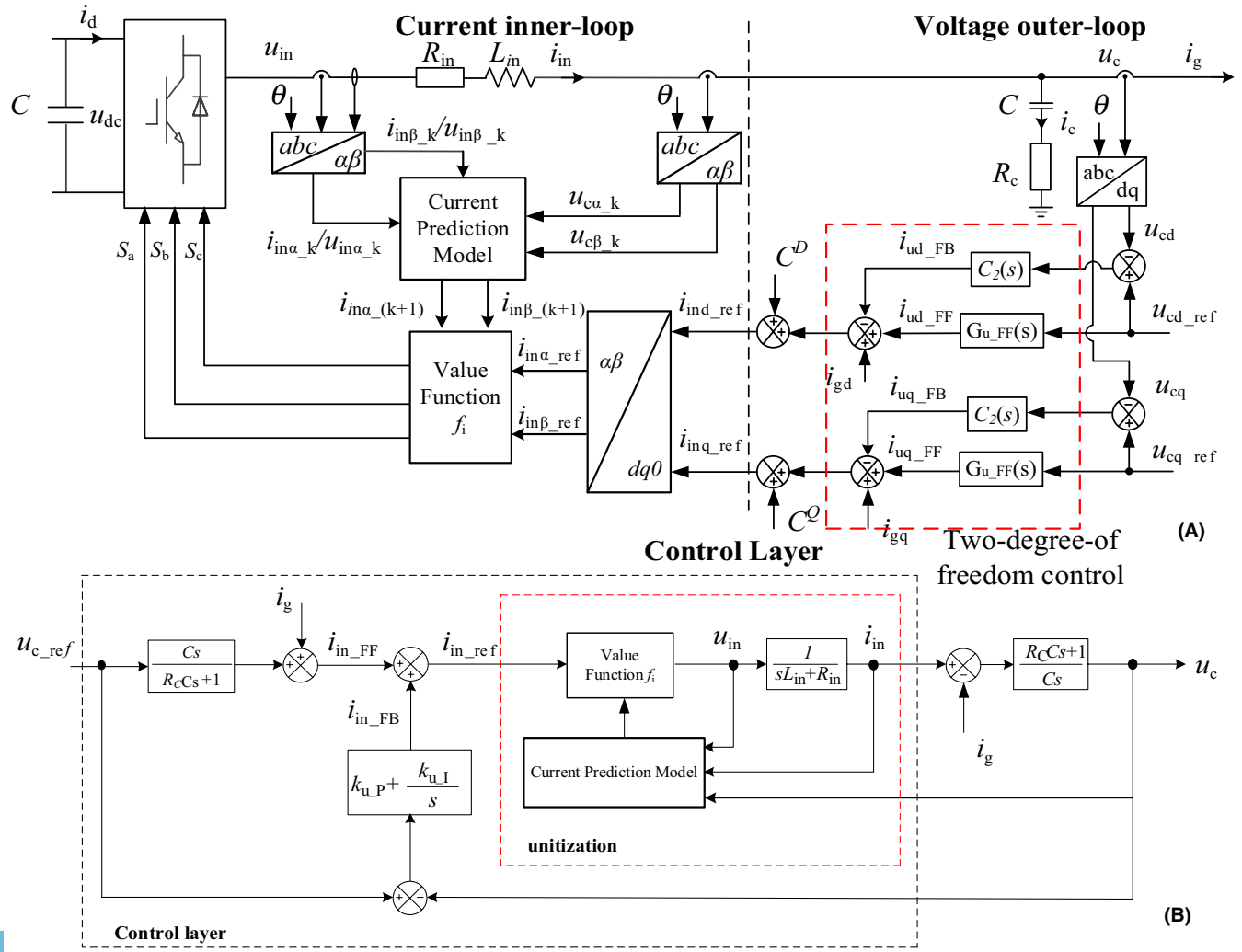

FIGURE 11 Structural block diagram of new control mode

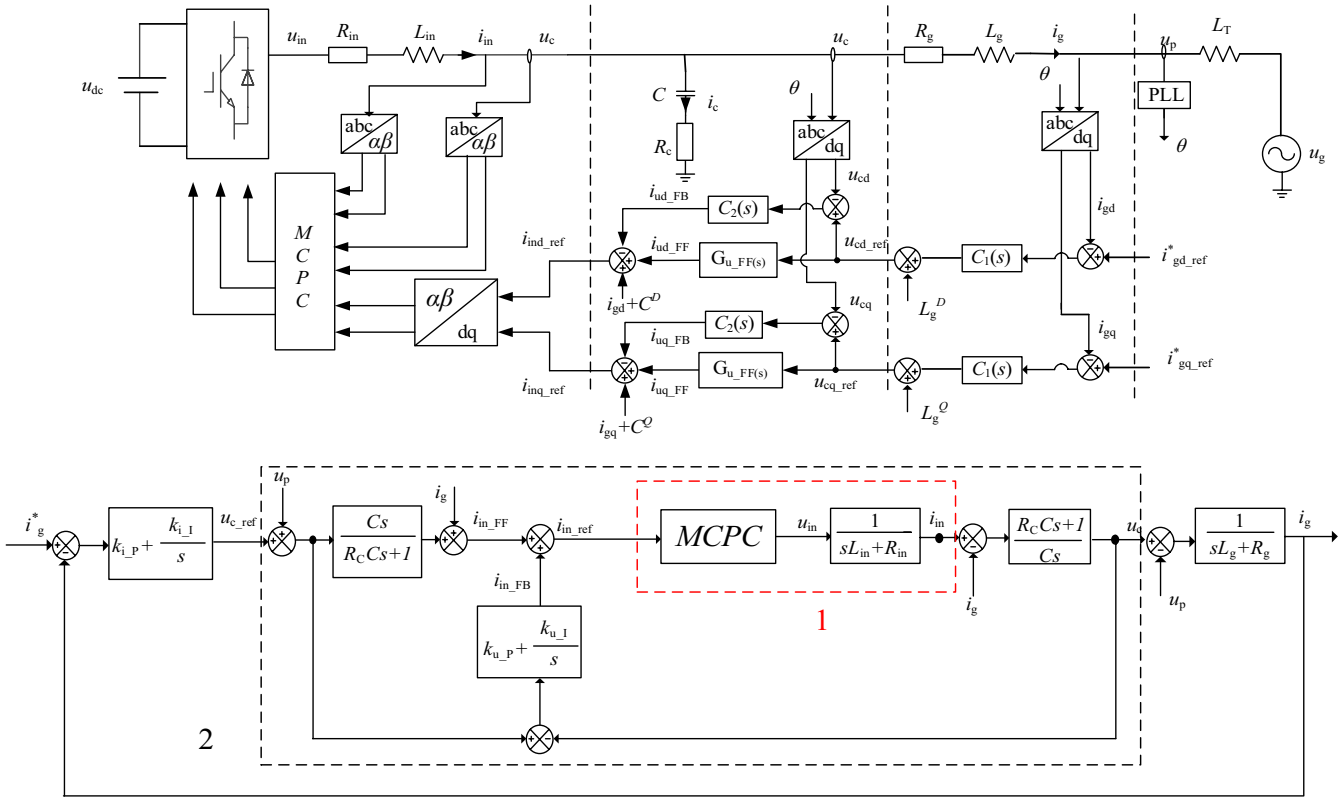

FIGURE 12 Structural block diagram of new control mode

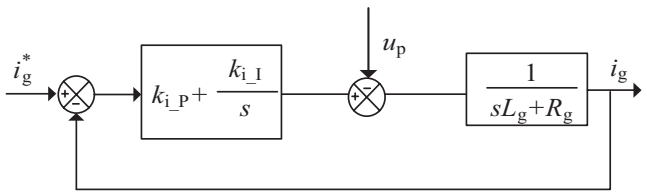

FIGURE 13 Control block diagram of novel control methods

possible grid-connected inverter switching state, the current predictions can be obtained from (13) and (15) considering voltage $u_{in\alpha}/u_{in\beta}$. The quality function of (14) is evaluated using the current predicted results. If, for a given switching state, the evaluated quality function f is stored as f_i, that lower value is stored as f_i, and the switching state number is stored as S_i. The loop ends when all eight switching states have been evaluated. The state that produces $f_{\min}$ is identified by the variable $S_{\min}$ and will be applied to the inverter during the next sampling interval, starting the MCPC algorithm again. Therefore, the inverter switching state can be obtained, making the output current the closest to its reference value.

3.2 | Model mismatched stability analysis of MCPC algorithm

In,[31-33] Lyapunov's second method is used to analyze the stability of MCPC. However, they are all without considering model errors. Therefore, if modeling errors exist, MCPC's stability needs further discussion.

Based on (14), because of $R_{in}T_s/L_{in} \ll 1$, the following equation can be obtained:

$$i_{in(k+1)} = \frac{T_s(u_{in\alpha\_k} - u_{c\alpha\_k})}{L_{in}} + i_{ink} \tag{16}$$

According to,[33] if the current errors of MCPC algorithm converge to a compact set which can be expressed as:

$$\Omega = \left\{ e \mid \|e\| \le \left(\frac{T_s}{L_{in} + R_{in}T_s} \right) (\phi + \varepsilon) \right\} \tag{17}$$

It can be obtained that the closed-loop system with MCPC algorithm can be regarded as practically exponentially stable. Here, e is error of predicting current, constant ϕ and ε are the upper bound of the quantization error vector and the estimation error of back-emf vector, respectively. Considering $R_{in}T_s/L_{in} \ll 1$, (17) can be simplified as:

$$\Omega = \left\{ e \mid \|e\| \le \frac{T_s}{L_{in}} \varphi \right\} \tag{18}$$

Here, $\varphi = \phi + \varepsilon$. According to (16) and (18), if the actual value and MCPC set value of inductance respectively are L_{inreal} and L_{in}, the error of prediction current can be defined as:

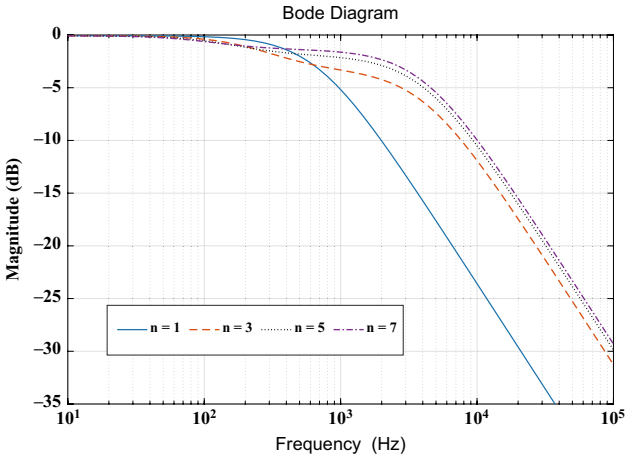

(A) Internal resonance Bode diagram of multi -inverter parallel System

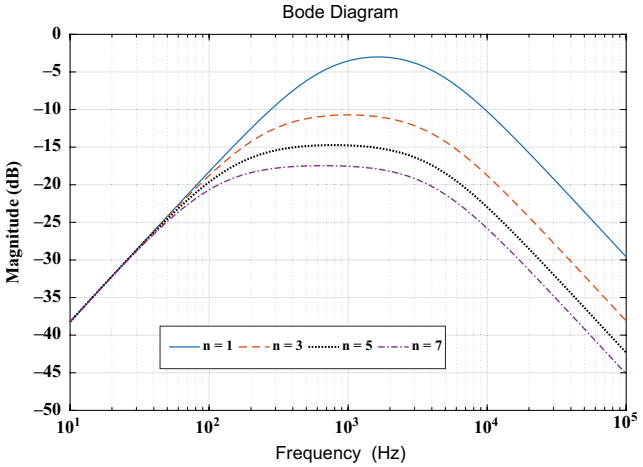

(B) Serial resonance Bode diagram of inverter parallel system

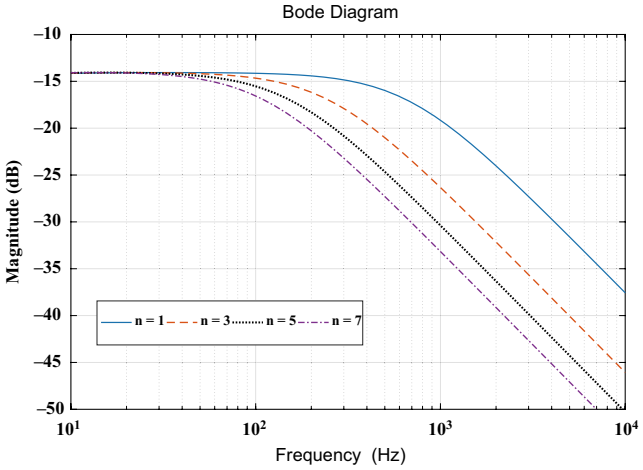

(C) Power system background harmonic series resonance Bode diagram

FIGURE 14 Resonance Bode diagram with novel method. (A) Internal resonance Bode diagram of multi-inverter parallel system. (B) Serial resonance Bode diagram of inverter parallel system. (C) Power system background harmonic series resonance Bode diagram

$$\begin{aligned}\left\|e_{real}(k+1)\right\| &= \left\|i_{in}^{*}(k+1)-i_{inreal}(k+1)\right\| \\ &= \left\|\left(1-\frac{L_{in}}{L_{inreal}}\right)(i_{in}^{*}(k+1)-i_{in}(k))-\frac{T_s}{L_{inreal}}\varphi\right\| \\ &\le \left\|\left(1-\frac{L_{in}}{L_{inreal}}\right)(i_{in}^{*}(k+1)-i_{in}(k))\right\|+\left\|\frac{T_s}{L_{inreal}}\varphi\right\| \\ &\approx \left\|\left(1-\frac{L_{in}}{L_{inreal}}\right)e(k)\right\|+\left\|\frac{T_s}{L_{inreal}}\varphi\right\| \\ &\le \left|1-\frac{L_{in}}{L_{inreal}}\right|\ \|e(k)\|+\frac{T_s}{L_{inreal}}\varphi\end{aligned} \tag{19}$$

According to (19), when $L_{in} < L_{inreal}$, the following conclusion can be obtained:

$$\begin{cases} 0<\left|1-\dfrac{L_{in}}{L_{inreal}}\right|<1 \\ \dfrac{T_s}{L_{inreal}}\varphi<\dfrac{T_s}{L_{in}}\varphi \end{cases} \tag{20}$$

Therefore, the current error is continuously decaying, and it will converge to a compact set which can be expressed as:

$$\Omega_1=\left\{ e|\ \|e\|\le\frac{T_s}{L_{inreal}}\varphi \right\} \tag{21}$$

Comparing (18) with (21), it can be found that in the case of $L_{in} < L_{inreal}$, Ω_1 is smaller than Ω, so that system's stability can still be guaranteed. When $L_{inreal} < L_{in} < 2L_{inreal}$, the following conclusion can be obtained:

$$\begin{cases} 0<\left|1-\dfrac{L_{in}}{L_{inreal}}\right|<1 \\ \dfrac{T_s}{L_{inreal}}\varphi>\dfrac{T_s}{L_{in}}\varphi \end{cases} \tag{22}$$

According to (22), the current error is also continuously decaying, and it will also converge to a compact set which can be expressed as:

$$\Omega_2=\left\{ e|\ \|e\|\le\frac{T_s}{L_{in}}\varphi \right\} \tag{23}$$

Then, it can be found that system still remain stable.

Considering that inductor's parametric variation is usually bounded within ±10%, so that the proposed method in this paper can meet the control requirements.

3.3 | Design of control layer outer loop

Figure 10 shows the block diagram of the two-degree-of-freedom control.[28] Here, $R(s)$, $Y(s)$, $C(s)$, $G_{FF}(s)$, $P(s)$, and

FIGURE 15 Bode diagram of $Z_g(s)/Z_{out}(s)$

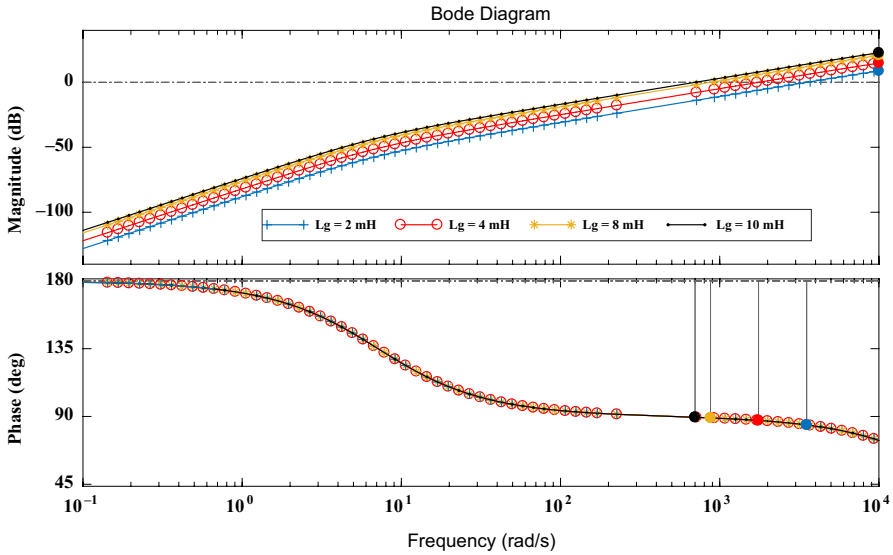

TABLE 2 Element parameters of control method

Parameters with traditional method		Parameters with novel method	
L_{in}	1.3 mH	L_{in}/R_{in}	1.3 mH/0.15 Ω
L_g	0.2 mH	L_g/R_g	0.2 mH/0.05 Ω
C	20 uF	C/R_c	20 uF/0.2 Ω
L_T	2 mH	L_T	2 mH
K_p	10	k_{i_P}	5
K_c	10	k_{i_I}	50
K_R	200	k_{u_p}	10
ω_c	5	k_{u_I}	50

$D(s)$ are the input signal, output signal, feedback controller, feedforward controller, controlled object, and disturbing signal, respectively. $E(s)$ is the error between input and output signals. From Figure 10, the transfer functions between $R(s)$ and $Y(s)$, $R(s)$, and $E(s)$ are[28]

$$\begin{cases} Y(s)=\dfrac{C(s)P(s)+G_{FF}(s)P(s)}{1+C(s)P(s)}R(s)+\dfrac{P(s)}{1+C(s)P(s)}D(s) \\ E(s)=\dfrac{\left[1-P(s)G_{FF}(s)\right]}{1+C(s)P(s)}R(s) \end{cases} \tag{24}$$

If $G_{FF}(s)=[P(s)]^{-1}$, (5) can be amended as:

$$\begin{cases} Y(s)=R(s)+\dfrac{P(s)}{1+C(s)P(s)}D(s) \\ E(s)=\dfrac{0}{1+C(s)P(s)}R(s) \end{cases} \tag{25}$$

Therefore, a unitary gain in all frequencies band can be obtained from the transfer function between $R(s)$ and $Y(s)$. And through regulating $C(s)$, $D(s)$ optimal control can be performed.

From the outer loop of control layer perspective, together with MPCP, the inner-loop reference current and inverter's output current be approximatively regarded as equal, so that their transfer function can be regarded as unitization (namely $i_{in}^*/i_{in}=1/(T_s+1)\approx 1$).[34-36] Therefore, according to Figure 10 and (24), if C is set as controlled object, in order to unitize the transfer function between reference voltage, u_{c_ref}, and capacitor voltage, u_c, the voltage outer loop of control layer is designed as Figure 11 shown. From Figure 11, the feedforward and feedback outputs signals are as follows:

$$\begin{cases} \begin{bmatrix} i_{ind\_FF} \\ i_{inq\_FF} \end{bmatrix}=G_{u\_FF}(s)\begin{bmatrix} u_{cd\_ref} \\ u_{cq\_ref} \end{bmatrix}+\begin{bmatrix} i_{gd} \\ i_{gq} \end{bmatrix} \\ \begin{bmatrix} i_{ind\_FB} \\ i_{inq\_FB} \end{bmatrix}=C_2(s)\begin{bmatrix} u_{cd\_ref}-u_{cd} \\ u_{cq\_ref}-u_{cq} \end{bmatrix} \\ G_{u\_FF}(s)=\dfrac{Cs}{R_cCs+1} \\ C_1(s)=k_{u\_p}+\dfrac{k_{u\_I}}{s} \end{cases} \tag{26}$$

Here, k_{u_p} and k_{u_I} are the proportional and integral gain of the outer loop feedback controller, respectively. L_{in} and C are the inductance and capacitance of the LC filter, respectively. R_{in} and R_c are the resistors associated with L_{in} and C, respectively. C^D/C^Q is the decoupling terms of C on the d/q axes. Then, according to (26), the equation, $u_c^*/u_c=1$, can be realized.

3.4 | Design of application layer

Based on the aforementioned control layer structure, owing to most DGs operate in the mode of current source, the decoupling impedance $Z_g=R_g+jwL_g$ is added. And together

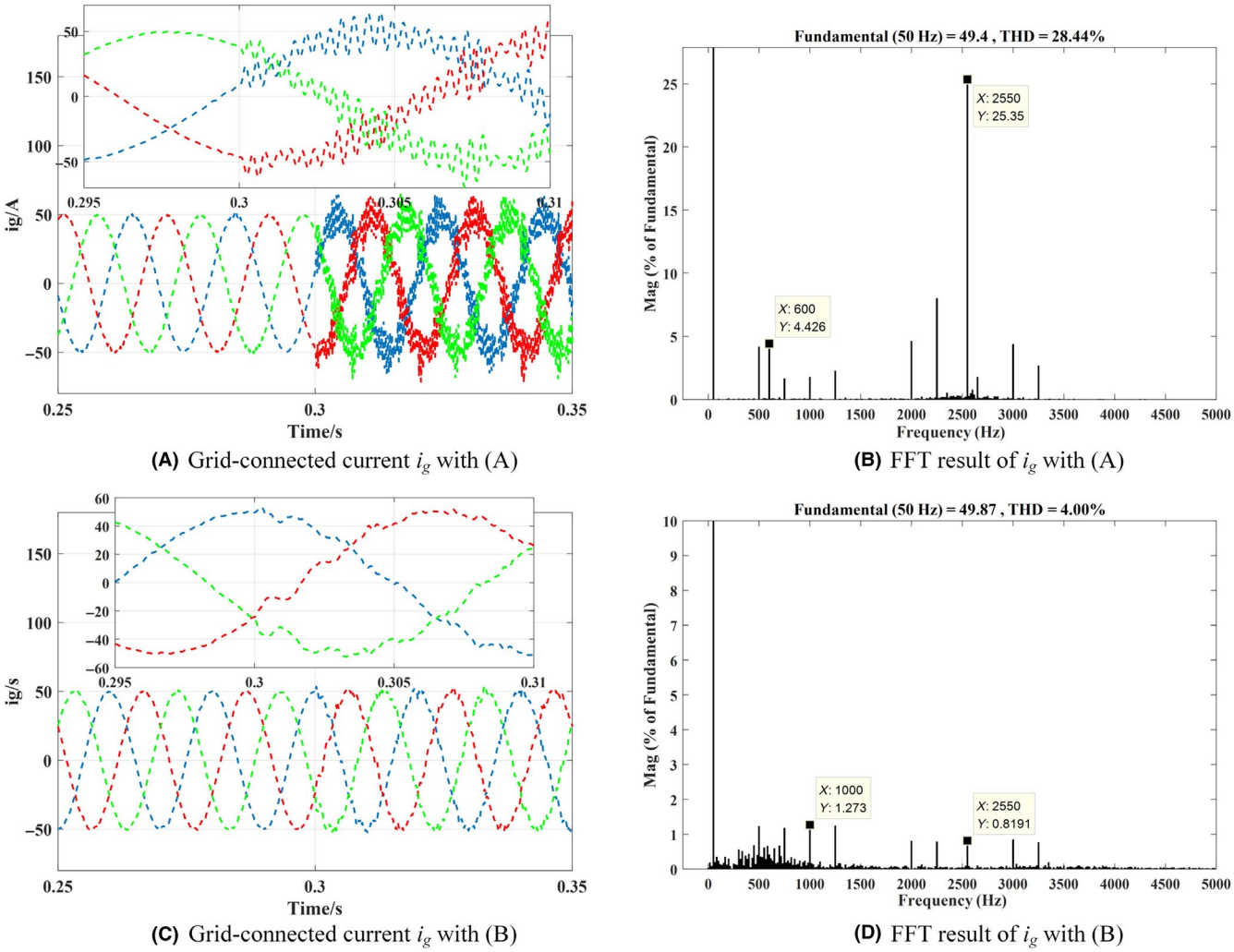

(A) Grid-connected current i_g with (A)

(B) FFT result of i_g with (A)

(C) Grid-connected current i_g with (B)

(D) FFT result of i_g with (B)

FIGURE 16 Simulation results of internal resonance

with *LC* type filter, it can realize the harmonic suppression function of *LCL*-type filter. Then, the control layer reference voltage u_{c_ref} is

$$\begin{bmatrix} u_{cd\_ref} \\ u_{cq\_ref} \end{bmatrix} = \begin{bmatrix} u_{pd} \\ u_{pq} \end{bmatrix} + \begin{bmatrix} R_g i_{gd\_ref} \\ R_g i_{gq\_ref} \end{bmatrix} + \left(k_{i\_P} + \frac{k_{i\_I}}{s} \right) \begin{bmatrix} i_{gd\_ref} - i_{gd} \\ i_{gq\_ref} - i_{gq} \end{bmatrix} \tag{27}$$

Here, $u_{pd}/u_{pq,}$ and i_{gd_ref}/i_{gq_ref} represent the *d*/*q* axis component of the grid-connected voltage and reference current, respectively. R_g and L_g are the decoupling resistance and inductance, respectively. k_{i_P} and k_{i_I} are proportional and integral gains of PI controller. According to (27) and Figure 11, the control block diagram of the novel control method as Figure 12 shown can be obtained. Here, L_g^D and L_g^Q are the decoupling terms of L_{in} on the *d*/*q* axes. From Figure 12, because of $i_{in\_ref}/i_{in} = 1$ and $u_{c\_ref}/u_c = 1$, the dynamic compensation is formed between the power grid voltage/inverter output current u_p/i_g and the introduced signal u_p/i_g.

3.5 | Amplitude frequency characteristics of novel control methods

Figure 13 shows the control block diagram of novel control methods. From Figure 13, the control coefficient of the controlled source, $G_i(s)$, and the inverter's output equivalent admittance, $Y_i(s)$, can be expressed as:

$$\begin{cases} G_i(s) = \dfrac{i_g}{i_g^*}\Big|_{u_p=0} = \dfrac{k_{i\_P}s + k_{i\_I}}{L_2 s^2 + (R_g + k_{i\_P})s + k_{i\_I}} \\ Y_i(s) = \dfrac{-i_g}{u_p}\Big|_{i_g^*=0} = \dfrac{s}{L_2 s^2 + (R_g + k_{i\_P})s + k_{i\_I}} \end{cases} \tag{28}$$

Comparing (28) with (3), it can be found that the order and its difference between numerator's highest order term and denominator's highest order term of $G(s)$ and $Y_i(s)$ are obviously decrease.

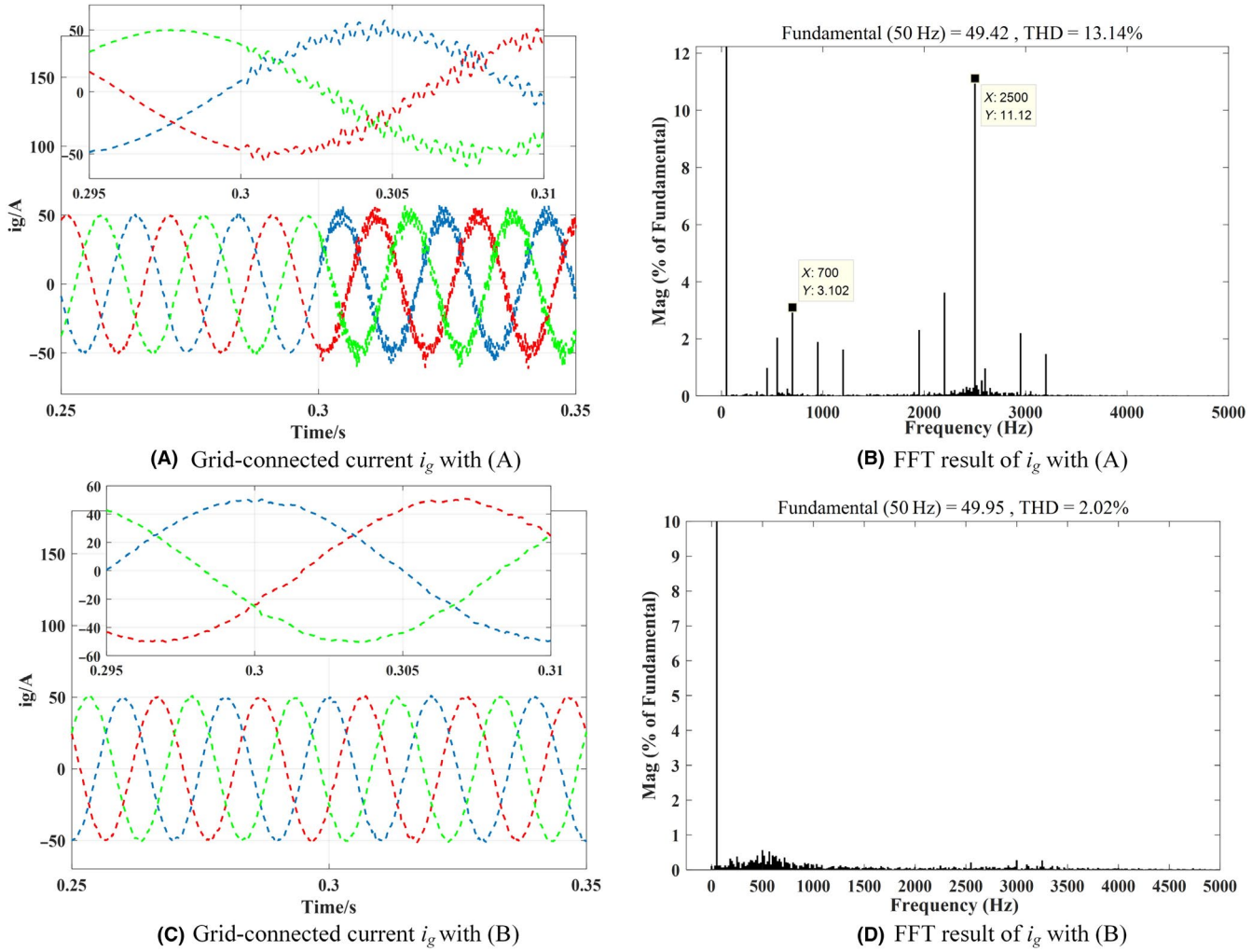

(A) Grid-connected current i_g with (A)

(B) FFT result of i_g with (A)

(C) Grid-connected current i_g with (B)

(D) FFT result of i_g with (B)

FIGURE 17 Simulation results of parallel resonance

According to (5)-(7), Figure 14A-C shows the resonance Bode diagram with this novel method. From Figure 14, with three type resonance sources, there is no peak value in their resonance transfer function and their gains all present attenuation effects, so that the resonance problems of multi-inverter parallel system can be eliminated.

3.6 | System stability analysis

According to,[37-39] in the proposed control model, there are two factors for affecting the control system instabilities in the weak grid case, namely PLL and grid-side voltage feedforward. However, PLL can be seen as a low-pass term, so that PLL mainly affects the amplitude frequency characteristics of the control system at low frequency. In this paper, the resonance frequency is usually thousands of Hz. Therefore, it is to ignore the interference from PLL in the proposed model.

Since voltage feedforward is introduced into the control layer, the stability of the system needs to be analyzed. According to,[40] three conditions need to be met for the system to maintain stability:

1. The current source itself is stable when unloaded, that is, when the load is a short-circuit ($Z_g = 0$)
2. The power grid is stable when supplied by an ideal current source
3. $Z_g(s)/Z_{out}(s)$ meets the stability criterion.

Here, Z_g is the equivalent impedance of the grid and $Z_{out} = 1/Y_i(s)$ is the equivalent impedance of the inverter. Both (1) and (2) can be satisfied, only (3) needs to be analyzed.

$$\frac{Z_g(s)}{Z_{out}(s)} = \frac{L_T s^2}{L_2 s^2 + (R_g + k_{i\_P})s + k_{i\_I}} \tag{29}$$

According to (29), the Bode diagram with different L_g can be draw, as Figure 15 shows. Based on Figure 15, when the

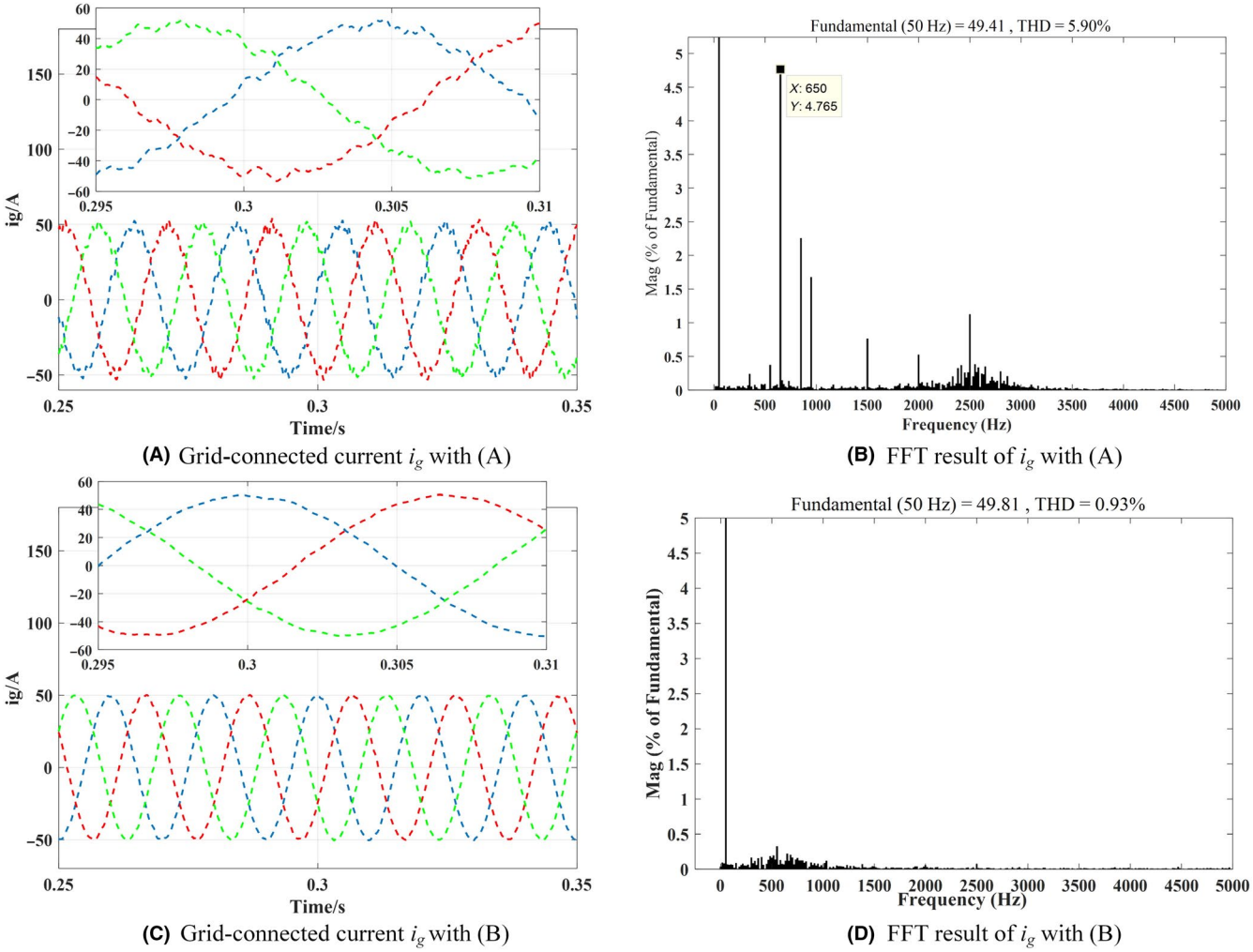

(A) Grid-connected current i_g with (A)

(B) FFT result of i_g with (A)

(C) Grid-connected current i_g with (B)

(D) FFT result of i_g with (B)

FIGURE 18 Simulation results of series resonance

equivalent impedance of the power grid changes in a large range, the phase angle margin of $Z_g(s)/Z_{out}(s)$ is still very large, indicating that the system can maintain stability.

4 | SIMULATION AND ANALYSIS

In order to assess the proposed method's performance, based on Figure 3 ($n = 3$) and Figure 12, a simulation model was constructed in MATLAB/SIMULINK. Table 2 lists the simulation parameters. Two different control methods were compared. These two control methods included (A) Traditional method,[41] (B) Proposed method.

4.1 | Simulation of internal resonance

In order to simulate the internal resonance of multi-inverter parallel system, at the time of 0.3 seconds, a series of 10th-65th harmonics are injected into the reference current of the first inverter.

The magnitude of harmonics with respect to the reference current is 3%. Simulation results can be seen in Figure 16. According to Figure 16A,B, after the time of 0.3 seconds, the grid-connected current waveform has been severely distorted with traditional method, and the THD value of i_g is 28.44%. It can be found that the harmonics with different frequency are all be amplified. The harmonics with a frequency of 600 Hz are amplified to 4.426%, and the harmonics with a frequency of 2550 Hz are amplified to 25.35%, which verified that the gain of high-frequency resonance is larger than the gain of low-frequency resonance in internal resonance.

After employing the novel method (B), the resonance suppression ability of the inverter is greatly enhanced, as shown in Figure 16C,D. The distortion of the grid-connected current's waveform is small. The THD of i_g is reduced to 4%, and all harmonics exhibit attenuation characteristics.

4.2 | Simulation of parallel resonance

To simulate the parallel resonance of multi-inverter parallel system, the first and second inverters are adopted to analyze the interaction between inverters on their resonance characteristics. At the time of 0.3 seconds, harmonics are added to the reference current of second inverter; then, the first inverter's grid-connected current and its FFT results are shown in Figure 17. As can be seen from Figure 17A, due to the injection current of the second inverter, the i_g is significantly distorted with traditional method (A). According to the FFT result in Figure 17B, the THD value of i_g is 13.14% and the harmonics with the frequency of 2550 Hz is amplified to 11.12%. While, according to Figure 17C,D, the waveform of i_g is basically not distorted with the novel method (B), all the harmonics are well suppressed, and the THD value of grid-connected current is reduced to 2.02%.

4.3 | Simulation of grid background harmonic series resonance

Here, the 13rd-50th harmonics are injected into the grid voltage, u_g, and the magnitude of the injected harmonic is 3%, with respect to the fundamental u_g. It can be seen in Figure 18A that the waveforms of i_g are distorted in traditional method (A). The measured *THD* of the waveforms of i_g shown in Figure 18B is 5.90%. However, according to Figure 18C,D, the i_g is perfectly sinusoidal under the novel method, and the FFT results show that the novel method is effective in suppressing the series resonance.

5 | CONCLUSION

According to MCPC and two-degree-of-freedom control, this paper proposes a novel control method for removing multi-inverter parallel system resonance. Based on a theoretical analysis and simulation verification, the following conclusions can be drawn:

1. Compared with traditional methods, the inner-loop PI controllers and PWM module can all be removed when using the proposed method.
2. When faced three type resonance sources (reference current changing in the inverter control system, reciprocal effect among multi-inverters, and grid background harmonic), through the MCPC and two-degree-of-freedom control, the grid-connected inverter is very effective in suppressing the resonances, and the quality of the grid-connected current is well guaranteed.
3. Through MCPC and two-degree-of-freedom control, the control layer can be recognized as unity gain, so that the dynamic full compensation of the disturbance (power grid voltage and inverter output current) can be realized and its influence on the control layer of multi-inverter parallel system can be removed.
4. The multi-inverter parallel system's simulation platform is established by MATLAB/Simulink. Simulation results verified that the proposed method can successfully suppressing the resonance problem of multi-inverter parallel system compared to traditional method.

ORCID

Feng Zheng https://orcid.org/0000-0001-9630-8699

REFERENCES

1. Rolán A, Giménez P, Yagüe SJ, Bogarra S, Saura J, Bakkar M. Voltage recovery influence on three-phase grid-connected inverters under voltage sags. *IET Gener Transm Distrib*. 2019;13(3):435-443.
2. Li Y, Dong P, Liu M, Yang G. A distributed coordination control based on finite-time consensus algorithm for a cluster of DC microgrids. *IEEE Trans Power Syst*. 2019;34:2205-2215.
3. Saim A, Houari A, Guerrero JM, Djerioui A, Machmoum M, Ahmed MA. Stability analysis and robust damping of multiresonances in distributed-generation-based islanded microgrids. *IEEE Trans Ind Electron*. 2019;66:8958-8970.
4. Zhao J, Xu Z, Wang J, Wang C, Li J. Robust distributed generation investment accommodating electric vehicle charging in a distribution network. *IEEE Trans Power Syst*. 2018;33:4654-4666.
5. Wu Y, Guerrero JM, Wu Y. Distributed coordination control for suppressing circulating current in parallel inverters of islanded microgrid. *IET Gener Transm Distrib*. 2019;13(7):968-975.
6. Sangwongwanich A, Yang Y, Sera D, Soltani H, Blaabjerg F. Analysis and modeling of interharmonics from grid-connected photovoltaic systems. *IEEE Trans Power Electr*. 2018;33(10):8353-8364.
7. Meyer R, Mertens A. Design and optimization of LCL filters for grid-connected converters[C]. International Power Electronics & Motion Control Conference. IEEE. 2012;S1a-S7a.
8. Liu Q, Peng L, Kang Y, Tang S, Wu D, Qi Y. A novel design and optimization method of an LCL filter for a shunt active power filter. *IEEE Trans Ind Electron*. 2014;61(8):4000-4010.
9. He J, Li YW, Bosnjak D, Harris B. Investigation and active damping of multiple resonances in a parallel-inverter-based microgrid. *IEEE Trans Power Electr*. 2013;28(1):234-246.
10. Gomes CC, Cupertino AF, Pereira HA. Damping techniques for grid-connected voltage source converters based on LCL filter: an overview. *Renew Sustain Energy Rev*. 2018;81:116-135.
11. Ye J, Shen A, Zhang Z, Xu J, Wu F. Systematic design of the hybrid damping method for three-phase inverters with high-order filters. *IEEE Trans Power Electr*. 2018;33(6):4944-4956.
12. Yang Q, Li K, Zhao C, Wang H. The resonance suppression for parallel photovoltaic grid-connected inverters in weak grid. *Int J Autom Comput*. 2018;15(6):716-727.
13. Wu W, He Y, Tang T, Blaabjerg F. A new design method for the passive damped LCL and LLCL filter-based single-phase grid-tied inverter. *IEEE Trans Ind Electron*. 2013;60(10):4339-4350.

14. Balasubramanian AK, John V. Analysis and design of split-capacitor resistive-inductive passive damping for LCL filters in grid-connected inverters. *IET Power Electron*. 2013;6(9):1822-1832.
15. Ben Said-Romdhane M, Naouar MW, Slama-Belkhodja I, Monmasson E. Robust active damping methods for LCL filter-based grid-connected converters. *IEEE Trans Power Electron*. 2017;32(9):6739-6750.
16. Xin Z, Wang X, Loh PC, Blaabjerg F. Grid-current-feedback control for LCL-filtered grid converters with enhanced stability. *IEEE Trans Power Electron*. 2017;32(4):3216-3228.
17. Perez-Estevez D, Doval-Gandoy J, Yepes AG, Lopez O, Baneira F. Enhanced resonant current controller for grid-connected converters with LCL filter. *IEEE Trans Power Electr*. 2018;33(5):3765-3778.
18. Pan D, Ruan X, Bao C, Li W, Wang X. Optimized controller design for LCL -type grid-connected inverter to achieve high robustness against grid-impedance variation. *IEEE Trans Ind Electron*. 2015;62:1537-1547.
19. Dannehl J, Liserre M, Fuchs FW. Filter-based active damping of voltage source converters with LCL filter. *IEEE Trans Ind Electron*. 2011;58(8):3623-3633.
20. Pena-Alzola R, Liserre M, Blaabjerg F, Sebastian R, Dannehl J, Fuchs FW. Systematic design of the lead-lag network method for active damping in LCL-filter based three phase converters. *IEEE Trans Industr Inf*. 2014;10:43-52.
21. Pena-Alzola R, Liserre M, Blaabjerg F, Ordonez M, Kerekes T. A self-commissioning notch filter for active damping in a three-phase LCL -filter-based grid-tie converter. *IEEE Trans Power Electron*. 2014;29(12):6754-6761.
22. Wang X, Ruan X, Liu S, Tse CK. Full feedforward of grid voltage for grid-connected inverter with LCL filter to suppress current distortion due to grid voltage harmonics. *IEEE Trans Power Electron*. 2010;25(12):3119-3127.
23. Shen G, Zhu X, Zhang J, Xu D. A New feedback method for PR current control of LCL-filter-based grid-connected inverter. *IEEE Trans Ind Electron*. 2010;57(6):2033-2041.
24. Yang D, Ruan X, Wu H. Impedance shaping of the grid-connected inverter with LCL filter to improve its adaptability to the weak grid condition. *IEEE Trans Power Electr*. 2014;29(11):5795-5805.
25. Xu J, Xie S. Current control based on zero-placement strategy for grid-connected LCL-filtered inverters[C]. Melbourne, VIC: IEEE ECCE Asia; 2013:1157-1162.
26. Vazquez S, Rodriguez J, Rivera M, Franquelo LG, Norambuena M. Model predictive control for power converters and drives: advances and trends. *IEEE Trans Industr Electron*. 2017;64:935-947.
27. Seifi K, Moallem M. An adaptive PR controller for synchronizing grid-connected inverters. *IEEE Trans Ind Electron*. 2019;66(3):2034-2043.
28. Wang J, Monti A. Current control of grid connected inverter with LCL filter utilizing two degree-of-freedom control[C]. International Conference on Renewable Energy Research & Applications. IEEE. 2013:967-972.
29. Zhang X, Tan L, Xian J, Zhang H, Ma Z, Kang J. Direct grid-side current model predictive control for grid-connected inverter with LCL filter. *IET Power Electron*. 2018;11(15):2450-2460.
30. Lee CT, Hsu CW, Cheng PT. A low-voltage ride-through technique for grid-connected converters of distributed energy resources. *IEEE Trans Ind Appl*. 2011;47(4):1821-1832.
31. Makhamreh H, Sleiman M, Kukrer O, Al-Haddad K. Lyapunov-based model predictive control of a PUC7 grid-connected multilevel inverter. *IEEE Trans Industr Electron*. 2019;66:7012-7021.
32. Parvez Akter M, Mekhilef S, Mei Lin Tan N, Akagi H. Modified model predictive control of a bidirectional AC–DC converter based on Lyapunov function for energy storage systems. *IEEE Trans Industr Electron*. 2016;63:704-715.
33. Kwak S, Yoo S, Park J. Finite control set predictive control based on Lyapunov function for three-phase voltage source inverters. *IET Power Electron*. 2014;7:2726-2732.
34. Rodriguez J, Pontt J, Silva CA, et al. Predictive current control of a voltage source inverter. *IEEE Trans Ind Electron*. 2007;54(1):495-503.
35. Cortes P, Ortiz G, Yuz JL. Model predictive control of an inverter with output LC filter for UPS application. *IEEE Trans Industr Electron*. 2009;56:1875-1883.
36. Xia C, Tao L, Shi T, et al. A simplified finite-control-set model-predictive control for power converters. *IEEE Trans Industr Inf*. 2017;10:991-1002.
37. Xu J, Qian Q, Zhang B, Xie S. Harmonics and stability analysis of single-phase grid-connected inverters in distributed power generation systems considering phase-locked loop impact. *IEEE Trans Sustain Energy*. 2019;10:1470-1480.
38. Chen X, Zhang Y, Wang S, Chen J, Gong C. Impedance-phased dynamic control method for grid-connected inverters in a weak grid. *IEEE Trans Power Electron*. 2017;32:274-283.
39. Xu J, Xie S, Tang T. Improved control strategy with grid-voltage feedforward for LCL-filter-based inverter connected to weak grid. *IET Power Electron*. 2014;7:2660-2671.
40. Sun J. Impedance-based stability criterion for grid-connected inverters. *IEEE Trans Power Electron*. 2011;26:3075-3078.
41. Keqing Q, Wenqi L, Jinbin Z, Tiankai Y, Xuhui C. A control strategy in a stationary frame for grid-connected inverter with LCL filter. In: *IET Conference Proceedings*; 2015. 2015-01-01.

How to cite this article: Zheng F, Lin X, Zhang Y, Deng C. Design of a novel hybrid control strategy for multi-inverter parallel system for resonance suppression. *Energy Sci Eng*. 2020;8:2878–2893. https://doi.org/10.1002/ese3.706

AUTHOR BIOGRAPHIES

Feng Zheng was born in Wen Zhou, Zhe Jiang, China in 1983. He received the BS and MS degrees in electric engineering from the Three Gorges University, China, in 2006 and 2009, respectively, and the PhD degree in electric engineering from Wuhan University, China, in 2017. Currently, he is a lecturer in School of Electrical Engineering and Automation at Fuzhou University. His main research interests include renewable energy fault ride through, and microgrid operation and control.

Xiangqun Lin was born in Sanming, China, in1996. He received the B.S degree in electrical engineering in 2019 from the College of Electrical Engineering and Automation, Fuzhou University, Fuzhou, China, where he is currently working toward the MS degree. His research interests include suppression for resonance of grid-connected inverters in Micro-grid.

Yachao Zhang received the B.S and MS degrees in water conservancy and hydropower engineering from Huazhong University of Science and Technology, Wuhan, China, in 2007 and 2010, respectively, and the PhD degree in electrical engineering from Wuhan University, Wuhan, China, in 2017. Currently, he is a lecturer in School of Electrical Engineering and Automation at Fuzhou University. His main research interests include power system optimization dispatch with renewable energy and wind power forecast.

Changhong Deng received the PhD degree from the School of Electrical Engineering, Wuhan University, Wuhan, China, in 2007, where she is currently a Professor. Her research interests include power system security and stability analysis, optimal control theory, and renewable energy integration.